COMPONENT PART NOTICE

THIS PAPER IS A COMPONENT PART OF THE FOLLOWING COMPILATION REPORT:

TITLE: Transonic and Supersonic Phenomean in Turbomachines: Proceedings of the Propulsion and Energetics (68th)(B) Specialists' Meeting Held in Munich, Germany on 10-12 September 1986.

TO ORDER THE COMPLETE COMPILATION REPORT, USE AD-A182 996.

THE COMPONENT PART IS PROVIDED HERE TO ALLOW USERS ACCESS TO INDIVIDUALLY AUTHORED SECTIONS OF PROCEEDING, ANNALS, SYMPOSIA, ETC. HOWEVER, THE COMPONENT SHOULD BE CONSIDERED WITHIN THE CONTEXT OF THE OVERALL COMPILATION REPORT AND NOT AS A STAND-ALONE TECHNICAL REPORT.

THE FOLLOWING COMPONENT PART NUMBERS COMPRISE THE COMPILATION REPORT:

AD#: AD-P005 506 thru AD-P005 523. AD#: ______

AD#: ______ AD#: ______

AD#: ______ AD#: ______

Accession For	
NTIS GRA&I	☑
DTIC TAB	☐
Unannounced	☐
Justification	
By	
Distribution/	
Availability Codes	
Dist	Avail and/or Special
A-1	

WAKE AND SHOCK INTERACTIONS IN A TRANSONIC TURBINE STAGE

by

D.L.Schultz and A.B.Johnson
Dept. of Engineering Sciences
Oxford University
Oxford OX1 3PJ, UK

D.A.Ashworth and M.J.Rigby
Rolls Royce
Derby, UK

and

J.E.LaGraff
Syracuse University
N.Y., USA

Abstract

The strong trailing-edge shock waves from the nozzle guide vanes of transonic turbine stages can give rise to interactions with the downstream rotor which are significantly more severe than is the case with lower pressure ratio stages. It is therefore important to study such effects in detail both from the point of view of stage power output and more importantly from that of heat transfer rates. A study has been made of a transonic rotor profile in a static cascade in which the effect of shock wave interaction is simulated by means of an array of bars rotating at the correct speed and spacing upstream of the stationary rotor blades. Detailed heat transfer rate measurements made with rapid response gauges enable the wake and shock phenomena to be separated.

Nomenclature

C_2 - NGV exit velocity, relative bar velocity
C_t - Tangential (or true) chord
k - Thermal conductivity (W/mK)
$\dot{q}$ - Heat transfer rate (W/m²)
M - Isentropic Mach Number (based on local static pressure and inlet total pressure)
Nu - Nusselt Number
Re - Reynolds Number (based on inlet total conditions, isentropic exit Mach Number and tangential chord)
s - Blade surface perimeter
t - Time
T - Temperature (K)
Tu - Turbulence level = $u'/\bar{U}$
u' - Fluctuating velocity (m/s)
U - Velocity (m/s)
V - Rotor relative velocity, cascade inlet velocity
x - Surface distance from the leading edge stagnation point
y_b - Distance in the pitch-wise direction from the spanwise datum position
β - Gas angle (measured from the axial direction)

Subscripts

∞ - Freestream
o - Total
1,2 - Inlet, Outlet
meas - Measuring point
h,m,t - Hub, mean, tip (or tangential in chord definition)
rel - Relative bar condition

Introduction

The effects of unsteady flows caused by rotor blade/NGV interactions and the disturbance to the potential flow due to rotor blade motion are arousing increasing interest as attempts are made by turbine designers to improve their predictions of performance. Previous work by Doorly[1-3] and Dunn[4-10] has shown the significant effect of NGV-rotor interaction on heat transfer rates associated with the effect of the turbulent NGV wake on the rotor boundary layer as the blade passes through the wake. Doorly's studies have identified the fluid dynamic phenomena associated with the interaction employing a stationary linear cascade and an array of bars rotated off-axis upstream of the blades in such a way as to generate a set of wakes which pass over an instrumented stationary blade. Dunn's studies, on the other hand, involved a complete rotor behind an NGV ring. An extensive study of unsteady secondary flow vortices in a turbine rotor stage has been made by Binder et al.[11-12]. Laser two-focus velocimetry was used to track the distortion and migration of the NGV passage vortex as it passed through the rotor blade ring. Simultaneous measurements of mean velocity and turbulence level were made. It was found that the turbulence level arising from this vortex was raised considerably by the cutting action of the rotor blades and this effect was ascribed by Binder et al. to the break-up of the vortex itself. The experiments were carried out in a steady flow turbine rig so that the long sampling times required for accurate L2F measurements were readily attainable. Hodson[13] has also investigated the blade-wake interaction measuring unsteady blade pressures on a large-scale rotating rig in a manner similar to that at UTRC where Dring and his colleagues[14-15] have studied blade boundary layers using a rotor axis fixed hot wire anemometer.

The work reported in the present study has been carried out in a linear cascade of the blades of a transonic stage where the NGV exit Mach Number is generally higher than that used by Doorly or Dunn and in which the strong recompression shocks in the wake have a more important effect on the boundary layer and hence on the heat transfer rates. The rotor profile is the same as that currently fitted to the MIT transient blowdown facility described by Epstein et al.[16] so that direct comparisons will be possible between the two different approaches.

Experimental Apparatus

The measurements were carried out in the isentropic light piston cascade described by Schultz et al.[17], in which a short duration (~ 0.5 sec.) flow is produced at the correct full-scale engine Reynolds and blade exit Mach Numbers and at the correctly scaled gas/wall temperature ratio. The simulation employed, i.e. stationary rotor and moving wakes has advantages in terms of simplicity over the fully rotating experiment in so far as Schlieren techniques may be employed to locate shock waves and boundary layer separations (induced, it will be seen, by the incident shock wave). It must be emphasised, however, that the following effects are not simulated:

1. Temperature gradients in the wake due either to a film cooled NGV or the heat transfer to the vane as a whole.
2. The differential effects of buoyancy forces on the cooled wake and the mainstream flow.
3. Distortion of the NGV passage flow by the rotor blockage.
4. The influence of unsteady secondary flows over both the rotor root and the tip region.

The simulation is, in effect, valid only for mid-blade height flows but is believed to be valuable nevertheless in that it enables the relevant fluid dynamic phenomena to be isolated and studied in some detail. The arrangement of the linear cascade, the rotating disc and stranded steel cables is illustrated in Fig. 1(a). A more complete description is given by Ashworth et al.[18] and it suffices here to record that the aerodynamic design of the prototype cold air turbine in which a 61 blade rotor spins at 9004 RPM behind an NGV ring of 36 vanes is correctly simulated by having a disc carrying 16 radial bars (stranded cable) and a turbine scaling factor cascade/cold air turbine of 1.3247. The NGV trailing edge diameter was 1.2192 mm and the nearest suitable cable diameter of 1.6151 mm was chosen for convenience. The plane of the array of the bars was located 14.333 mm upstream of the cascade blade leading edge line. Experiments reported by Doorly[2-3] have shown that a wake velocity profile similar to that from an NGV can be produced by a circular cylinder of diameter equal to that of the vane trailing edge. The cascade has a span of 50 mm at blade inlet and 56.095 mm at exit with the expansion on one side only as illustrated in Fig. 1(a). A turbulence grid 208 mm upstream of the cascade provides a level of $u'/\bar{U}$ of approximately 3%. Upstream and downstream static and total pressures were measured routinely to establish the correct cascade operating conditions and are reported in more detail by Ashworth et al.[18]. The operating conditions at the nominal engine design point are given below.

The heat transfer gauges used in this study are conventional thin film surface resistance thermometers widely used for the determination of heat transfer rate in short duration facilities[19]. Data from 22 such gauges were stored in a digital transient recorder sampling up to 16 channels at 500 kHz for each channel or were input directly to the A/D converter at a slower rate of 400 Hz for some of the 64 available A/D channels when time average data only were required, also used for measurements such as inlet and exit static pressures. The locations of these heat transfer gauges on the blade are shown in Fig. 2(a) and given in terms of the surface length 'x' to perimeter 's' from the stagnation point. A more detailed study of the reaction of the suction surface boundary layer to both freestream turbulence and the wake-passing phenomena is also reported below. For this study another blade was instrumented with thin film gauges which were only 4 mm long as compared to 10 mm for the previous tests, and were more closely spaced around the profile, as shown in Fig. 2(b). The model points in Fig. 2(b) are those referred to in Fig. 6. Surface pressures were measured in a time-averaged manner using Sensym semiconductor transducers type LX-1620D operating in a differential mode as reported in more detail by Ashworth et al.[18]. Baseline experimental results have been reported by Ashworth et al. but for clarity some of this data is referred to in the present paper. The velocity triangle for the steady nominal design case is shown in Fig. 1(b) which includes the effect of the reduced NGV exit wake velocity C_2' on the rotor inlet angle β_1.

Experimental Results

Mean Heat Transfer Without Wake Interaction

A comparison of baseline data with no rotor/wake interaction is given in Fig. 3(a) for the two cases of low (< 0.8%) freestream turbulence and with a turbulence level of approximately 3%. It will be seen that the turbulence generated by the bar grid is sufficient to bring the region of boundary layer transition forward from about 60% x/s on the pressure surface and 50% x/s on the suction surface to 10% and 20% respectively. All of this data was taken at the nominal design cascade operating conditions:

$$T_{total} = 432\ K$$

$$M_{exit} = 1.18$$

(based on isentropic inlet total and pitchwise averaged exit static pressures)

$$Re = 0.919 \times 10^{6}$$

$$\beta_1 = 58.06°.$$

The circled numbers refer to heat transfer gauges identified in Fig. 2(a). The heat transfer rate is presented in terms of a non-dimensional Nusselt Number, defined as:

$$Nu = \frac{\dot{q}_{meas}}{(T_o - T_{meas})} \frac{C_t}{k}$$

Instantaneous and Mean Heat Transfer with Wake Interaction

The heat transfer rate to the blade with the additional effect of wake interaction is illustrated in Figs. 3(b) and 3(c) for both cases of effectively zero freestream turbulence and ~ 3% $u'/\bar{U}$. From Fig. 3(c) it will be seen that there is an overall increase in heat transfer rate over both the pressure and suction surfaces. The pressure surface heat transfer is enhanced over practically the whole length although the dominant effect is observed for values of x/s < 70%. On the pressure surface the effect of wake interaction persists to about x/s = 30%. Examples of instantaneous heat transfer rates are inset in the Figure and a more extensive 'atlas' of results is given in Ashworth et al.[18]. The heat transfer rates with wake interaction and with effectively zero freestream turbulence are shown in Fig. 3(b). As expected there is a marked increase in the level of heat transfer rate over almost the entire pressure and suction surfaces. Examples of instantaneous values of heat transfer rate are inset and these also illustrate the increase over the undisturbed case.

Mean Effects of Inlet Incidence Angle on Heat Transfer Rate and Pressure Distribution

As is illustrated in Fig. 1(b) the passage of the reduced velocity wake through the rotor blading gives rise to a time varying change of incidence angle. Although this change is associated with the blade-wake interaction there is nevertheless a time-averaged effect which leads to quite marked variations, particularly on the suction surface heat transfer rate and pressure distribution. Considering first the heat transfer rate, Fig. 4(a), illustrates the more prolonged region of laminar heat transfer rate associated with a decreased incidence of -10° from design value of 58.06°. Studies at an increased incidence of 63.06° were carried out for off-design performance purposes only and although reported here for reference are not a part of the overall wake-blade interaction experiments. The unsteady incidence effects caused by the wake velocity deficit are not correctly simulated by measurements made in the steady state but it is probable that the nature of the transient changes, at least near the leading edge, are in line with those shown. Similar remarks apply to the effect of a decreased incidence on Mach Number distribution around the blade, Fig. 4(b), the overall result being a reduction of Mach Number, i.e. unloading of the crown of the suction surface, $x/s < 40\%$.

Measurement of the Unsteady Disturbance at Inlet

In order to understand the unsteady phenomena caused by the bar-passing apparatus, a sketch of the expected inlet disturbances in the simulation and the engine is given in Fig. 5(a). The velocity triangles are matched by setting the correct bar velocity and matching the cascade inlet velocity to the rotor relative velocity. The intermittent perturbations to the inlet flow caused by the simulation are shown for the high freestream turbulence case in Fig. 5(b) in terms of hot-wire output from the probe mounted in the freestream inlet plane at mid-passage, and surface stagnation point measurements of pressure and heat transfer rate. Both these results and the detailed measurements on the suction surface are presented from tests using the bar-passing apparatus described above with just 2 bars fitted, as opposed to the 16 bars necessary to model the correct blade passing frequency of the cold-air turbine design. This enables individual bar-passing events to be separated in time, since it is difficult to tell whether events were merging together from the 16 bar experiments alone. This data is normalised with respect to 2 cycles of the bar-passing event, so that it is possible to relate information from different runs in terms of cycle fraction. The signals show a background turbulent level extending over about 60% of the cycle characterised by a similar type of signal to that obtained with no rotating bars. All three signals have a periodic component at bar-passing frequency with two characteristic parts:

(i) Over about 6% of the cycle rapid changes in level of the order of 5 to 10 μs rise and fall times are observed. The pressure signal varies by +/- 25% and the heat transfer rate by approximately +/- 50%. This disturbance is attributed to shock waves generated as the bar sweeps past the cascade. By examination of Schlieren photographs of this flow, examples of which are given in Fig. 7, the nature of the NGV simulated shock structure can be determined. Clearly two shocks are associated with one bar-passing event, the bow and recompression shocks that would be expected at the bar relative Mach Number in steady flow. The separation time between these shocks is approximately 75μs, marked as Δt_s in Fig. 5(b), and is seen to correspond to the time interval between the sharp falls in level to the adjacent sharp peak.

(ii) Following these rapidly changing events, a second less marked change in level associated with the wake is also visible over about 10% of the cycle, marked as the "wake" region in Fig. 5(b).

Time-Resolved Heat Transfer Rate Measurements on the Suction Surface

The nature of the reaction of otherwise laminar boundary layers to both a higher level of isotropic freestream turbulence, and to the intermittent disturbances caused by the wake and shock/boundary layer interactions was investigated in more detail using the instrumented suction surface shown in Fig. 2(b), and these results are presented in Fig. 6.

(a) Natural Transition of the Suction Surface Boundary Layer

Wide bandwidth heat transfer signals obtained from the surface thin film gauges clearly illustrate the important differences between the low and high freestream turbulence cases as shown in the high frequency traces of Fig. 6(a). There is a constant spacing of 5 mm between the thin film gauge results shown, starting with gauge 3 at an x/s value of 0.12 through to gauge 15 at x/c = 0.65. The low turbulence case (Run 5723) remains quiet (laminar) throughout the entire measuring range of the transient data (to x/c = 0.65). The surface heat transfer for the high freestream turbulence case, while starting somewhat higher than the laminar case, becomes increasingly dominated by sharp transient events (consistent with the theory of turbulent spot development, growth, and gradual merger as proposed by Emmons[16] and verified by many others (e.g. Schubauer and Klebanoff[21]). These spots, which raise the heat transfer coefficient instantaneously to high turbulent levels, continue to grow and merge until finally the Nusselt Number signals become increasingly characterised by the "steady" turbulent levels. It is clearly seen that by the x/s = 0.65 station the flow is at the turbulent level more than half of the time but drops precisely to the undisturbed laminar values between the turbulent events. In other tests conducted at 1.5 x Re design, the boundary layer was fully turbulent at this location.

The physical process of turbulent spot breakdown to turbulence can be seen in Fig. 6(a). The growth and rearward convection of individual turbulent spots is clearly seen as they move along the blade surface. The spot signals grow in height and width as the spots cover more of each succeeding thin film gauge and shift in time downstream. This breakdown process is quantified in more detail in Ashworth[22] where intermittency levels are estimated from the digital time records and spot convection rates are estimated from cross-correlation analysis of adjoining thin film signals.

(b) Detailed Wake and Shock Interaction Effects

It is possible to analyse the reaction of the blade boundary layer to the wake and shock perturbations with 2 bars rotating by investigation of the sequence of time-resolved Nusselt Number plots given in Fig. 6(b),(c) and (d). The high freestream turbulence case with wakes and shocks present (Fig. 6(b)) is markedly different to the naturally transitional boundary layer (Fig. 6(a)) over the first 35% of the surface, with similar rapid rises and falls in Nusselt Number to the perturbations evident in Fig. 5. This shock related event occurs on the early suction surface due to a shock/boundary layer interaction starting at gauge 9, close to the crown of the suction surface. Examination of the Schlieren photographs (Fig. 7) indicates that the shocks first interact with the boundary layer near to gauge 9, the reflection point moving towards the leading-edge as the bar moves in the same direction. This is visible on the early gauges on Fig. 6(b), occurring first on gauge 9 then moving gradually through gauges 7 and 5 and finally showing on gauge 3. The rapid drop in surface Nusselt Number is attributed to an unsteady separation and the rise to a turbulent re-attachment both caused by the shock boundary layer interaction. The effect of the wake is not clearly discernable in Fig. 6(b) and to aid in identification of this the bars were rotated at a lower speed such that the bar relative Mach Number was subsonic. The results of this are shown as Fig. 6(c) with a much more clearly identifiable enhancement in heat transfer due to this wake. This extends to the later gauges of the surface causing the boundary layer to be fully turbulent over the extent of the wake. In Fig. 6(d) the background turbulence was reduced to less than 0.8% and the periodic disturbances due to the bar-passing events are more clearly evident. The early suction surface has shock-related phenomena extending well into the cycle period with apparent oscillations in Nusselt Number moving with the shock. Also apparent from Fig. 6(d) is the intermittent nature of the turbulence induced in the boundary layer by the wake and shock interaction, as the boundary layer clearly returns to its undisturbed laminar value between the periodic events. The heat transfer enhancement due to the wake is clearly evident along the whole surface.

In summary, it appears that the state of the turbine boundary layer seems to be controlled by the level of freestream turbulence except during the time for which the shock and wake actually pass through the cascade passage.

Schlieren Photographs of the Wake and Shock Interaction

In Fig. 7 Schlieren photographs showing four passages of the cascade (marked A to D) are presented for five instants in the bar-passing cycle. This reflected Schlieren technique gives changes in tone corresponding to the integrated effects of density gradient across the span of the cascade, so that events running normal to the tunnel sidewall show up most clearly. With no bars present the general mid-tone appearance varies most at the trailing-edge shocks with some effects due to the high accelerations near to the leading-edges. The photographs in Fig. 7 are from the 2 bar tests, as the pictures become somewhat confusing in the high-frequency wake-passing case. The position of the bar is shown corresponding to time 1, 26 μs before the bar reaches its datum position at 90° to the tunnel sidewall. The tip of the bar enters and leaves the cascade when the bar radial line is inclined at +/- 45° to its datum position, but over the range of photographs shown this angle varies from -3° to 17° thus amounting to 11% of the cycle between bar-passing events. The shock and wake events are evident in all of these photographs so is detailed here for each of the times in Fig. 7:

1. The bow shock is visible in passage C as a thin horizontal line just touching the crown of the suction surface. The curved end of this shock is due to refraction from the leading-edge of the upper blade of this passage, as the shock was chopped here as the bar swept by, vertically downwards from the point of view of these photographs. Some weak shock activity is evident in passage D, as will be discussed below. Passage C contains some reflected shock activity associated with the bar recompression shock. The wake can be seen as a mottled region in passage A covering more than half of the passage.

2. 71μs later the bow shock has passed the lower blade leading-edge of passage C and is now being refracted from this point. The recompression shock is now in passage C, with its distorted shape due to reflection effects. The wake is now visible in both passages A and B.

3. After another 65μs the bow shock has nearly left the lower passage (D), with a quite strong reflected shock visible as a series of arcs, due to the three-dimensional nature of the shock as will be described below. The recompression shock is close to the leading-edge of the upper blade of passage D, also reflected across the passage. The wake is steadily encroaching in to the two upper passages (A and B).

4. The reflection of the recompression shock in passage C is still evident, and the refraction of the same shock in the lower passage is now overlapping with the reflection of the bow shock, which now also is reflecting again from the pressure surface. The wake is now starting to appear in passage C.

5. A short time (30μs) later the shock activity has almost cleared passage C, save for some weak secondary reflections of the recompression shock still evident, surprisingly reflecting again off the suction surface. It is assumed that these weaker shock interactions would not have much effect on the boundary layer state, but could cause some of the oscillations in heat transfer noticeable only in the cases where M_{rel} (the bar relative Mach Number corresponding to U_{rel}) is transonic.

Predictions of the Wake and Shock Positions

2-Dimensional Wake Predictions

For the five times corresponding to the Schlieren photographs shown in Fig. 7, predictions of the wake position were calculated, the results of which are shown in Fig. 8. The wake itself is almost 2-dimensional in form, varying mainly in height across the span due to the 3-dimensional bar geometry, so that only a 2-dimensional calculation is necessary. The procedure follows that described in Doorly**, now fully automated and allowing for the spreading of the wake by using a width proportional to the square-root of the distance from the bar along the line of U_{rel} with the constant of proportionality derived from a database of wake measurements. The prediction procedure is as follows:

(i) A prediction of the flowfield velocity is made, in this case using the Denton scheme[34] and stored by the program.

(ii) U_{rel} is calculated (assumed constant across the span), the center-line of the undistorted wake is calculated from the specified bar position and the width added.

(iii) The wake is shifted back in time so that the bar will return to its correct position following the marching process of the prediction routine.

(iv) From this initial position elements of the wake are convected by small time steps using the local velocity interpolated from the prediction until the bar reaches the specified location. The differential velocities in the flowfield cause distortion of the wake along its length and across its width as it is accelerated through the passage.

This simple scheme, which could be incorporated in the blade design process, agrees well with the positions of the wake on the Schlieren photographs, so that the fraction of time that the heat transfer rate to the surface is affected by the wake could be calculated and included in the intermittency term of a prediction. It also demonstrates that to the level of our measuring ability second-order effects such as the "negative jet" effect do not significantly effect the wake position, as referred to in Doorly[33], and that the assumption that this flow unsteadiness may be superimposed on the steady flowfield is a valid approximation.

Quasi-3-Dimensional Shock Prediction

Although it was possible to model the wake in 2-dimensional terms, the shock structure associated with the transonic nature of the bar (as M_{rel} varies from 1.06 at the hub to 1.25 at the tip) is not strictly 2-dimensional, as has been seen in the Schlieren photographs (Fig. 7). An attempt was made to predict the positions of the bow and recompression shocks due to the bar in order to allow trajectory rate calculations to be made relating to the heat transfer measurements, and to aid in understanding phenomena observed in the Schlieren photographs. An example of such a prediction is presented as Fig. 9. The prediction is based on the assumption that for a small element of the bar the flow is 2-dimensional with respect to the plane containing U_{rel} and normal to the bar axis, a quasi-3-dimensional approach described in detail in Ashworth[35]. As U_{rel} varies in both magnitude and direction, so does the associated shock structure, and unlike the wake, this variation should be accounted for. The method of prediction was computerised as follows:

(i) For assumed constant inlet conditions and a specified position of the bar M_{rel} is calculated and its direction determined.

(ii) The equation of the bow shock in the 2-dimensional plane described above is derived from M_{rel} using the method described in Shapiro[36], shock properties and turning angles obtained by curve-fit equations where necessary over a range of Mach Number from 1.0 to 1.5.

(iii) The recompression shock is assumed to be straight and inclined at the Mach angle ($\sin^{-1} 1/M_{rel}$) to the direction of M_{rel} with a virtual origin two diameters downstream of the bar.

(iv) The shocks are chopped and refracted if they are downstream of the blade axial leading-edge point, with allowance made for regeneration of the shock as it moves away from this point.

(v) Finally the points of intersection with the blade suction surface are calculated, and the shocks are simply reflected from an origin mid-way between the two intersection points.

Comparison with the Schlieren photographs is encouraging, the position shown in Fig. 9 corresponding to time 2 in Fig. 7., and it is hoped that information from this simplified model will prove useful as an aid to understanding the complex shock movements in turbine passages, in spite of the many simplifying assumptions made in this prediction (such as allowing for no variation of the freestream velocity).

Conclusions

It has been established during the course of this study that the Isentropic Light Piston Tunnel facility combined with the wide bandwidth/high sampling rate heat transfer instrumentation has proved capable of tracking very rapidly progressing unsteady events in a transonic boundary layer. Operating under a simulated unsteady gas turbine rotor environment, sensitive detection and precision tracking of transient shock, wake and boundary layer transitional events was accomplished.

A second major outcome of this study was the observation that the strong unsteady interaction of a double shock and a simulated NGV wake with the rotor boundary layer did not have any measurable "long-term" effects apart from the strong excursion in heat transfer associated with the actual passing of the shocks and wake. The heat transfer fluctuation levels were essentially unchanged far removed from the disturbance (in time) and nearly identical at the rearmost measuring point except for a turbulent patch associated with the shock/wake event itself.

The interaction of the shocks and wake with the rotor establishes in more detail the earlier observation of Ashworth et al.[19] and Doorly and Oldfield[1] of strong changes in local heat transfer coefficient. The tracking of the interaction over the surface could be followed with some precision with the time resolution of the instrumentation used.

Predictions of the positions of both the wake and shock structures caused by the bar are most encouraging, as they are based on simplified models easily incorporated in the design process, unlike many other methods which are to unwieldy for turbine designers to use. They both are based on superimposing the unsteady structures on existing steady-state information, and as such agree well with measured data.

Acknowledgements

This work has been carried out with the support of the Procurement Executive, Ministry of Defence, and also Rolls-Royce plc to whom the authors are grateful for permission to publish this paper. The authors wish to acknowledge the assistance of M. L. G. Oldfield and K. J. Grindrod during the experiments, and to thank Dr. J. D. Denton for providing his time-marching code. Professor LaGraff would also like to acknowledge the financial support of the U.S. Air Force Office of Scientific Research under grant number 85-0295 and the Division of International Programs of the National Science Foundation under grant number INT-8509407.

References

1. Doorly, D. .. and Oldfield, M. L. G., "Simulation of Wake Passing in a Stationary Turbine Rotor Cascade", J. Eng. for Gas Turbines and Power, ASME, Vol. 107, pp. 998-1006, 1985.

2. Doorly, D. J. and Oldfield, M. L. G., "Simulation of the Effects of Shock Wave Passing on a Turbine Rotor Blade", ASME Paper No. 85-GT-112, 1985.

3. Doorly, D. J., Oldfield, M. L. G. and Scrivener, C. T. J., "Wake Passing in a Turbine Rotor Cascade", AGARD CP-390, pp. 7.1-7.18, 6th May, 1985.

4. Dunn, M. G. and Hause, A., "Measurement of Heat Flux and Pressure in a Turbine Stage", ASME J. Eng. for Power, Vol. 104, pp. 215 223, 1982.

5. Dunn, M. G., Lukis, G., Urso, M., Haimanx, R. J., Orazulak, R. and Key, N. J., "Instrumentation for Gas Turbine Research in Short Duration Facilities", Aerospace Congress, Long Beach, CA, Paper No. 841504, 15th - 18th October, 1984.

6. Dunn, M. G., Rae, W. J. and Holt, J. L., "Measurement and Analysis of Heat-Flux Data in a Turbine Stage", Parts I and II, J. Eng. for Power, Vol. 106, No. 1, January, 1984.

7. Dunn, M. G., Martin, H. L. and Stanek, M. J., "Heat Flux and Pressure Measurements and Comparison with Prediction for a Low Aspect Ratio Turbine Stage", ASME Paper No. 86-GT-79.

8. Dunn, M. G., "Heat Flux Measurements for a Rotor of a Full-Stage Turbine: Part I - Time-Averaged Results", ASME Paper No. 86-GT-77.

9. Dunn, M. G., George, M. K., Rae, M. J., Woodward, S. M., Moller, J. C. and Seymour, P. J., "Heat-Flux Measurements for the Rotor of a Full-Stage Turbine: Part II - Description of Analysis Technique and Typical Time-Resolved Measurements", ASME Paper No 86-GT-78.

10. Dunn, M. G., "Experimental Measurements of Heat-Flux Distributions in a Turbine Stage with Upstream Disturbances", Advanced Earth-to-Orbit Propulsion Technology Conference, Huntsville, Alabama, 13th - 15th May, 1986.

11. Binder, A., Foerster, W., "Turbulence Production due to Secondary Vortex Cutting in a Turbine Rotor", ASME Paper No. 85-GT-13.

12. Binder, A., Foerster, W., Mach, K. and Rogge, H., "Unsteady Flow Interaction Caused by Stator Secondary Vortices in a Turbine Rotor", ASME Paper No. 86-GT-302.

13. Hodson, H. P., "An Inviscid Blade-to-Blade Prediction of Wake Generated Unsteady Flows", ASME Paper No.84-GT-189, 1984.

14. Dring, R. P. and Joslyn, H. D., "The Relative Eddy in Axial Turbine Rotor Passages", ASME Paper No. 83-GT-22, 1983.

15. Dring, R. P., Joslyn, H. D., Hardin, L. W. and Wagner, J. H., "Turbine Rotor-Stator Interaction", ASME J. Eng. for Power, Vol. 104, pp. 729-742, 1982.

16. Epstein, A. H., Guenette, G. R. and Norton, R. J. G., "The MIT Blowdown Turbine Facility", ASME Paper No. 84-GT-116, 1984.

17. Schultz, D. L., Jones, T. V., Oldfield, M. L. G. and Daniels, L. C., "A New Transient Cascade Facility for the Measurement of Heat Transfer Rates", AGARD CP-229, 1977.

18. Ashworth, D. A., LaGraff, J. E., Schultz, D. L. and Grindrod, K. J., "Unsteady Aerodynamic and Heat Transfer Processes in a Transonic Turbine Stage", ASME Paper No. 85-GT-128, 1985.

19. Schultz, D. L. and Jones, T. V., "Heat Transfer Measurements in Short Duration Hypersonic Facilities", AGARDOGRAPH No. 165, 1973.

20. Emmons, H. W., "The Laminar-Turbulent Transition in a Boundary Layer - Part I", J. Aero. Sci., Vol. 18, No. 7, July, 1951.

21. Schubauer, G. B. and Klebanoff, P. S., "Contributions on the Mechanics of Boundary Layer Transition", NACA Report 1289, 1956.

22. Ashworth, D. A., LaGraff, J. E., and Schultz, D. L., "Unsteady Interaction Effects on a Transitional Turbine Blade Boundary Layer", Paper to be presented at the Joint ASME/JSME Gas Turbine Conference, March, 1987.

23. Doorly, D. J., "A Study of the Effect of Wake Passing on Turbine Blades", D.Phil. Thesis, University of Oxford, 1983.

24. Denton, J. D., "An Improved Time-Marching Method for Turbomachinery Flow Calculation", ASME J. Eng. for Power, Vol. 105, pp. 514-520, 1983.

25. Ashworth, D. A., "Unsteady Wake and Shock Interactions on a Transonic Turbine Blade", D.Phil. Thesis, University of Oxford, 1986.

26. Shapiro, A. S., "The Dynamics and Thermodynamics of Compressible Fluid Flow", Ronald Press, Vol. 2, pp. 884-886, 1954.

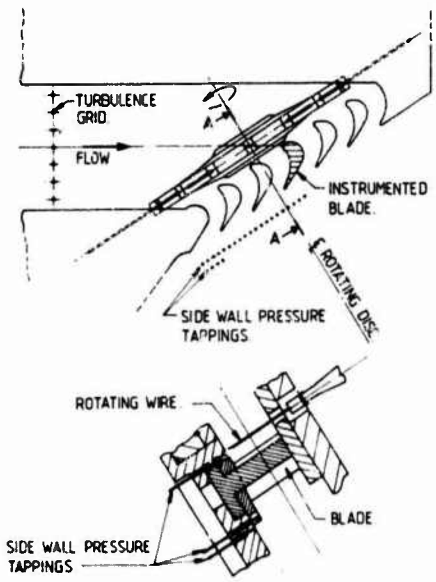

SECTION A-A.

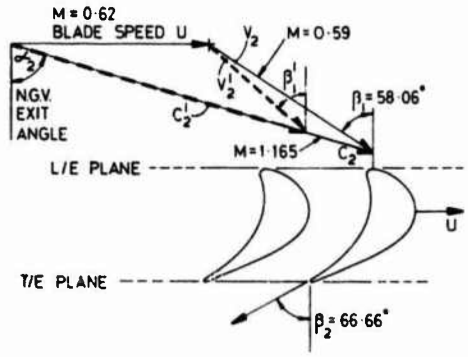

Fig. 1(a) Arrangement of the rotating bar wake generator and cascade.

Fig. 1(b) Velocity triangles at inlet for the steady nominal design case at mid-span, showing the reduced incidence caused by the deficit in the wake.

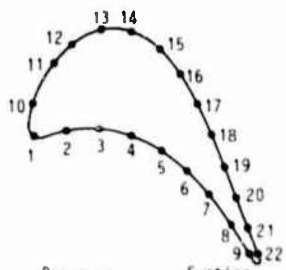

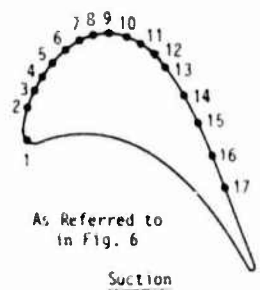

(a)

Pressure Surface Model Point	x/s	Suction Surface Model Point	x/s
1	0.00	10	0.08
2	0.12	11	0.14
3	0.24	12	0.24
4	0.36	13	0.31
5	0.48	14	0.38
6	0.59	15	0.46
7	0.71	16	0.53
8	0.84	17	0.61
9	0.96	18	0.68
		19	0.76
		20	0.83
		21	0.90
		22	0.96

(b)

Suction Surface Model Point	x/s
1	0.00
2	0.08
3	0.12
4	0.15
5	0.19
6	0.24
7	0.28
8	0.31
9	0.35
10	0.39
11	0.43
12	0.47
13	0.51
14	0.58
15	0.65
16	0.73
17	0.81

Fig. 2(a) Co-ordinates of the original heat transfer gauges on the blade profile.

Fig. 2(b) Co-ordinates of the heat transfer gauges for the detailed suction surface study, referred to in Fig. 6.

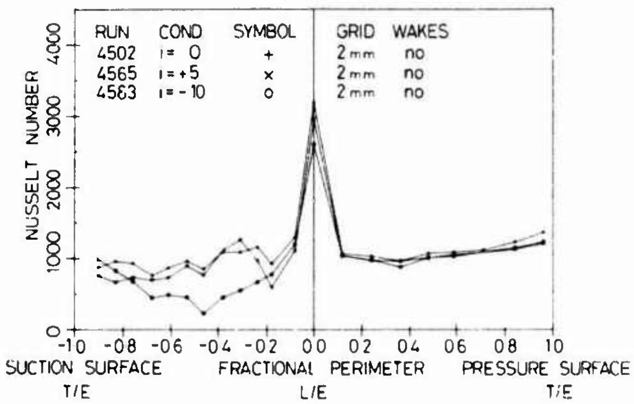

Fig. 4(a) Effect of incidence variation on mean heat transfer rate at the nominal design case (M_2 = 1.18, Re = 0.919E6) with no wake and shock interaction.

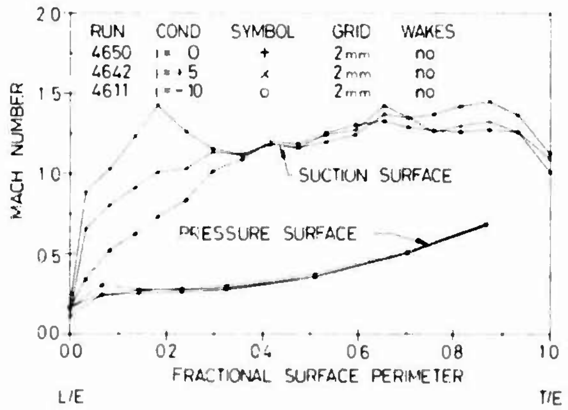

Fig. 4(b) Effect of incidence variation on mean surface isentropic Mach Number at the nominal design case (M_2 = 1.18, Re = 0.919E6).

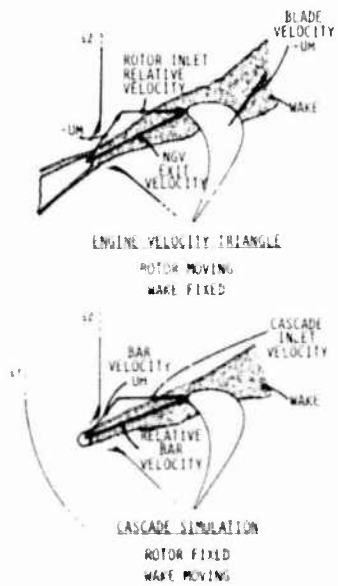

Fig. 5(a) Illustration of the comparative velocity triangles for the engine and cascade simulation of the NGV/rotor interaction.

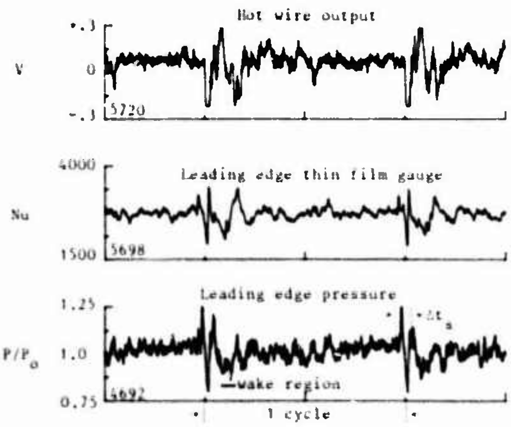

Fig. 5(b) Measurements of the unsteady disturbance at inlet by a hot-wire in the freestream and heat transfer and pressure measurements at the stagnation point.

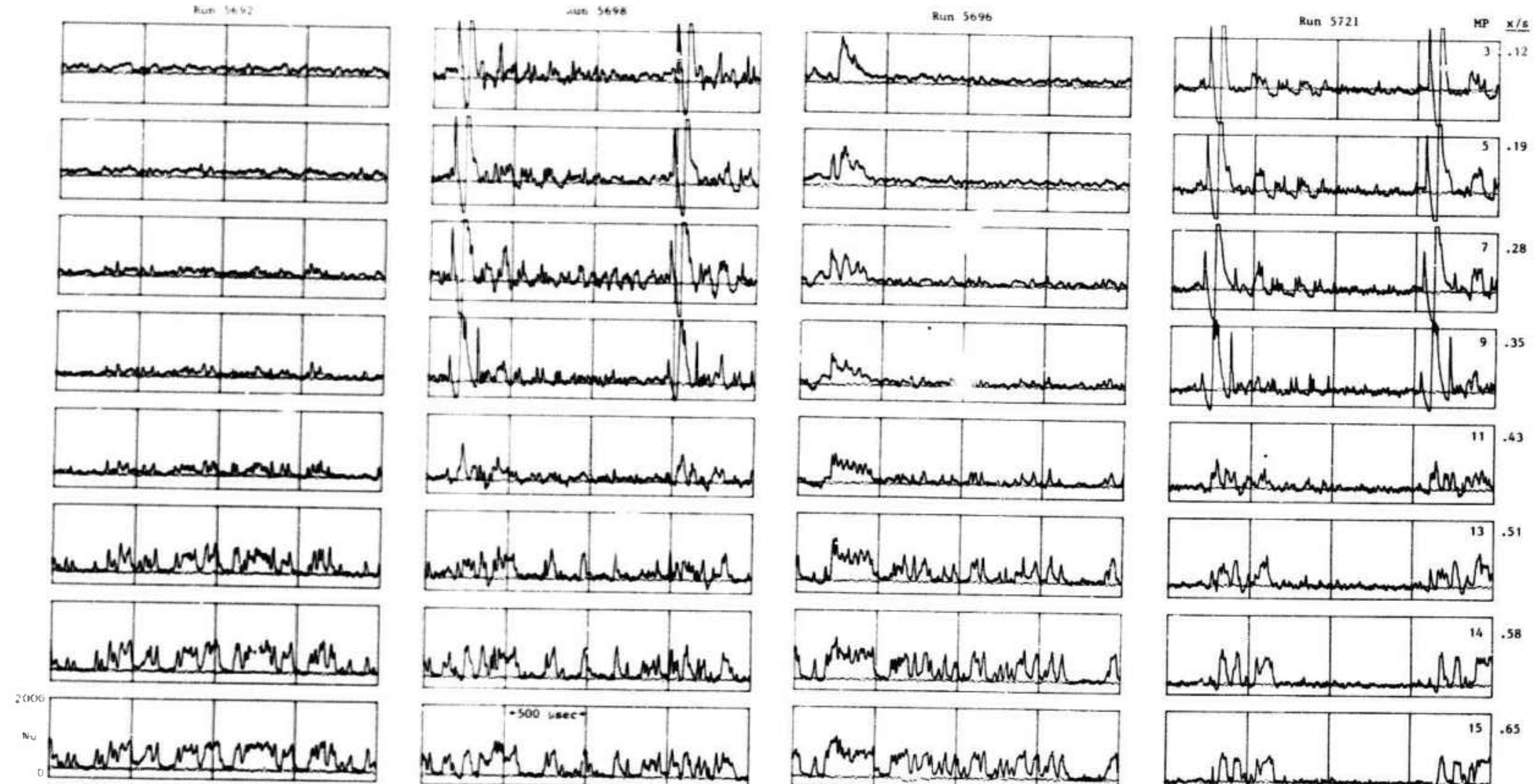

(a) Natural transition on the undisturbed boundary layer

(b) Shock and wake passing with high free-stream turbulence (≈ 3%)

(c) Wake passing only and high freestream turbulence (≈ 3%)

(d) Shock and wake passing with low free-stream turbulence (< 0.8%)

Fig. 6 Detailed time-resolved heat transfer rate measurements to the blade suction surface. The dotted lines are the baseline undisturbed results for the low freestream turbulence case (< 1%, Run 5723).

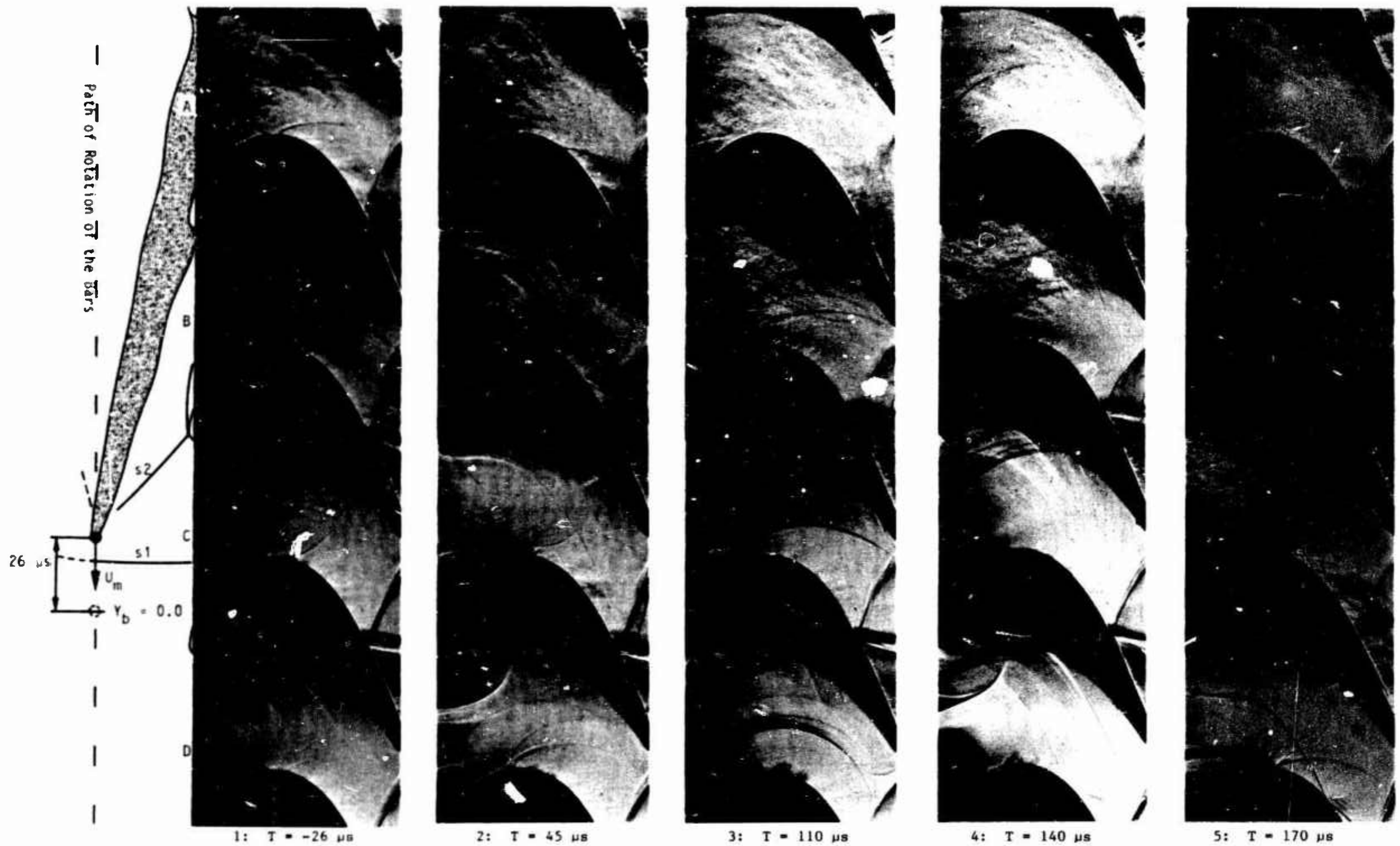

Fig. 7 Schlieren photographs of the cascade for different times in the bar-passing cycle. The position of the bar corresponding to time 1, the left-hand photograph, is illustrated with a sketch of the expected wake and shock positions (not visible in the photographs due to the limita of the Schlieren window).

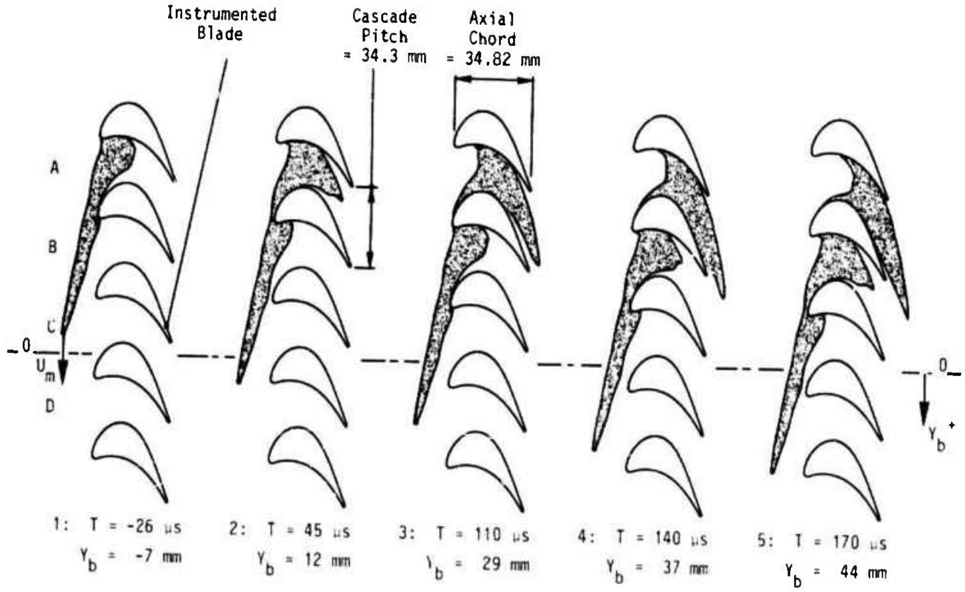

Fig. 8 Predicted wake positions at times corresponding to the Schlieren photographs in Fig. 7. The two lines for each time are the leading and trailing edges of the highly turbulent wake region.

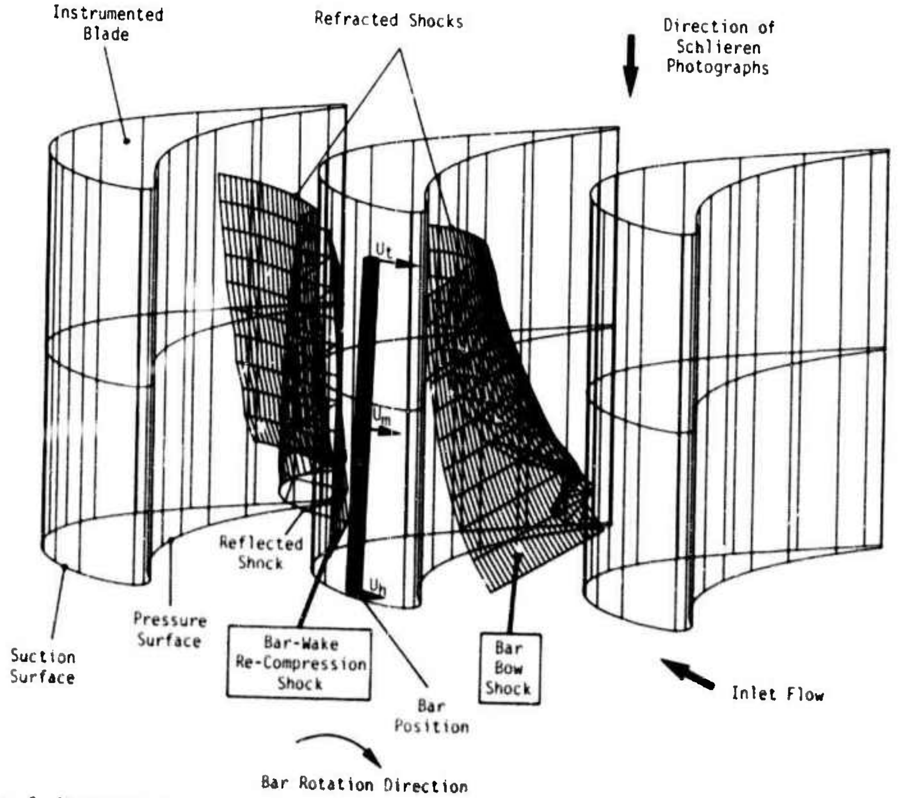

Fig. 9 Predicted shock position corresponding to time 2 of Fig. 7, with the bar inclined at ~ 2° to its datum position. Only the half of the shocks downstream of the bar are shown for clarity. The refraction and reflection of both shocks can be seen, with the re-compression shock more 2-dimensional in form than the detached bow shock, due to stand-off distance variation with bar relative Mach Number. Both shocks are weaker towards the hub due to the lower Mach Number there, with the bow shock strength less than the re-compression shock strength at each radius.

DISCUSSION

P.Ramette, Fr

The wake is induced, in your experiment, by a bar with a diameter corresponding to the nozzle trailing-edge section, which is symmetrical, while the nozzle wake is non-symmetrical. Consequently, you do not have the same gradients. How representative of a nozzle wake effect is your experiment?

Author's Reply

The work reported here is the follow-up of work carried out on a different profile, with a lower relative bar Mach Number, as reported by Doorly[27]. Prior to these tests, static tests were carried out by inserting a bar in a cascade with NGV's mounted in the same test section. It was therefore possible to traverse both bar and nozzle wakes and it was noted that the bar wake was quite representative of the NGV wakes. The larger momentum deficit corresponding to the suction side boundary layer that one would expect to contribute to the asymmetry did not appear to be significant and we assumed the same to be true for our cascade. It is worth noting that the weaker shock in the experiments reported by Doorly[1-3] only caused a boundary separation once the shock passed the leading edge of the blade. It is very interesting that quite different results can be obtained from similar experiments with only a few parameters altered, the most important of which is the shock strength.

[27] Doorly, D.J., "A Study of the Effect of Wake Passing on Turbine Blades", D.Phil Thesis, University of Oxford, 1983.